

Plasma generation by ultrashort multi-chromatic pulses during nonlinear propagation

Jeremy R. Gulley, Jiexi Liao, and Thomas E. Lanier

Department of Biology and Physics, Kennesaw State University, 1000 Chastain Rd.,
Kennesaw, GA 30144, USA

ABSTRACT

The use of femtosecond lasers in industrial, biomedical, and defense related applications during the last 15 years has necessitated a detailed understanding of pulse propagation coupled with ultrafast laser-material interactions. Current models of ultrashort pulse propagation in solids describe the pulse evolution of fields with broad spectra and are typically coupled to models of ionization and laser-plasma interaction that assume monochromatic laser fields. In this work we address some of the errors introduced by combining these inconsistent descriptions. In particular, we show that recently published experiments and simulations demonstrate how this contradiction can produce order-of-magnitude errors in calculating the ionization yield, and that this effect leads to altered dimensions and severity of optical breakdown and laser-induced modifications to dielectric solids. We introduce a comprehensive treatment of multi-chromatic non-equilibrium laser-material interaction in condensed matter and successfully couple this model to a unidirectional (frequency-resolved) pulse propagation equation for the field evolution. This approach, while more computationally intensive than the traditional single rate equation for the free electron density, reduces the number of adjustable phenomenological parameters typically used in current models. Our simulation results suggest that intentionally multi-chromatic fields (i.e. strongly chirped pulses or co-propagating pulses of different frequencies) can be arranged to control ionization yields and hence ultrafast laser induced material modifications.

Keywords: Ultrashort laser pulses, pulse propagation, plasma generation, ionization

1. INTRODUCTION

Ultrafast nonlinear pulse propagation and laser-induced ionization in bulk media are interrelated research areas with broad and promising applications. A correct understanding of propagation effects combined with laser-material interaction is critical for progress in bulk micro-machining, remote sensing, laser-induced breakdown spectroscopy, and laser-based medical procedures.¹⁻⁴ To elucidate the physics of these applications, one must simultaneously model the propagation of the laser field and its interaction with the material.^{5,6} These combined areas of research also present a challenge for theoretical calculations, due in large part to the computing requirements of combining fully 3D pulse propagation simulations with detailed calculations of laser-plasma dynamics. Each of those calculations are cumbersome individually, and combining them typically involves using a detailed model of one process and a simplified model of the other. An accurate coupling of the two will require a fully comprehensive model of both that are self-consistent in their approximations. However, the current simulations coupling ultrafast laser-material interactions with pulse propagation contain many inconsistencies and oversimplifications.⁷

Laser-induced ionization and interactions with the laser-generated electron-hole plasma are two of the basic effects that play a role in high-power ultrafast propagation in solids.^{5,8} The current understanding of photoionization and laser-generated plasma interactions is based on models derived in the decades preceding ultrafast laser pulse systems. As such, they are built on the assumption of plane wave-like monochromatic radiation. The current approach to couple laser-plasma interactions with pulse propagation is to replace the constant electric field amplitude of the monochromatic approximation using a time-dependent pulse amplitude, keeping the single-frequency approximation for the pulse spectrum.^{5,6,8} While this works well for pulses with narrow spectra,

Further author information: (Send correspondence to Jeremy R. Gulley)
Jeremy R. Gulley: E-mail: jgulley@kennesaw.edu, Telephone: 1 678 797 2933

Frontiers in Ultrafast Optics: Biomedical, Scientific, and Industrial Applications XIV, edited by Alexander Heisterkamp,
Peter R. Herman, Michel Meunier, Stefan Nolte, Proc. of SPIE Vol. 8972, 89720T
© 2014 SPIE · CCC code: 0277-786X/14/\$18 · doi: 10.1117/12.2040666

Proc. of SPIE Vol. 8972 89720T-1

a pulse with a duration approaching one optical cycle cannot be accurately represented in this way. It is also inconsistent with computational propagation schemes that utilize a more realistic spectral representation of the pulse and thus accommodate arbitrary pulse spectra. Only a fully time-resolved (not time-averaged) description of laser-plasma interactions will be adequate for such simulations, but there are currently no laser-solid interaction models of sufficient simplicity for coupling with the already computationally intensive pulse propagation calculations.

This problem is further complicated by the fact that the laser-plasma models currently coupled to pulse propagation in solids neglect many of the most important behaviors of carrier dynamics. This is particularly significant when the laser field drives the electron distribution far from its equilibrium configuration. Pulse propagation simulations in dielectrics typically limit their laser-plasma models to a single rate equation for the conduction band electron density,^{8,9} or in some recent cases a multi-rate equation for the same purpose.¹⁰⁻¹⁴ These models use either semi-classical or phenomenological approaches for laser energy absorption by the carriers and are coupled to pulse propagation via a local Drude model. Theorists specifically concerned with the evolution of these non-equilibrium distributions use quantum kinetic models to include many-body effects involving carrier collisions with laser photons, impurities, phonons, and other electrons.¹⁵⁻¹⁷ To achieve greater fidelity to the fundamental physics of carrier scattering dynamics, pulse propagation simulations in the future should model laser-plasma interactions in dielectric solids with models based on the quantum kinetic approaches often used to study semiconductors. The main obstacle to coupling these more accurate solid-state models with pulse propagation is that the combined computational demands of both models typically exceed available computing resources. The refinement of material models applicable to self-consistent simulations of ultrafast high-power pulse propagation is an active field of study. This work presents recent progress towards such an approach.

2. THEORY

In dielectrics and semiconductors, the electron-hole plasma results from electron transitions from the valence band to the conduction band, initially by photoionization. In bulk solids this is typically modeled with monochromatic approaches, such as the ones derived by Keldysh¹⁸ and others.^{19,20} Although widely used for ultrashort pulses, such monochromatic approaches for photoionization do not properly represent the photoionization of multi-chromatic fields, as one finds in strongly chirped pulses or simultaneous two-frequency multi-pulse trains. Once in the conduction band, electrons may absorb laser energy nonlinearly and can transfer it to valence-band electrons via collisions producing impact ionization. Sequential single-photon absorption events result in a delayed development of the impact ionization as shown by simulations using the Boltzmann¹⁷ and Fokker-Planck²¹⁻²³ equations and then incorporated into single and multi-rate equations.^{10,12} However, these models of free-carrier dynamics to date are also monochromatic. This approximation ignores the fact that the multi-chromatic spectrum of ultrashort laser pulses must spread the electron-energy distribution function as electrons absorb laser energy.

In most pulse propagation simulations, the time-evolved carrier density from a rate equation model is exported to a Drude model for the free current density that assumes averaged values for material constants such as collision rates and effective carrier masses.^{8,24-28} Since collision rates and effective masses are known to vary significantly as functions of electron energy,²⁹ the free-carrier transport must sensitively depend on both the spectral components of the laser pulse and the conduction band energy (or momentum) at which laser photons are absorbed or emitted. Furthermore, both experiment and pulse propagation equations demonstrate that the energy absorbed by the plasma from ultrashort pulses varies as a function of the instantaneous intensity slope and pulse chirp.³⁰⁻³² In this work we present a comprehensive theoretical framework in which to overcome these limitations in some cases and specify the limits of its applicability.

2.1 Photoionization

For the simulations presented in this paper, a modified Keldysh photoionization rate for solids¹⁸ is used because in numerous studies it has provided good agreement with experiments of ultrashort laser pulse propagation in fused silica,^{17,24,28,33-39} the material studied in this work. The Keldysh photoionization formula for a field of

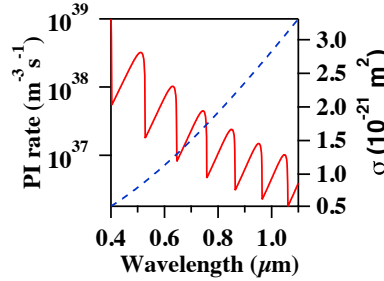


Figure 1. Photoionization rate for an intensity of 5×10^{12} W/cm² in fused silica calculated by Eq. 1 (solid line, left axis) and the inverse-Bremsstrahlung absorption coefficient (dashed line, right axis) for a collision time of 1.2 fs, both as functions of laser wavelength. Additional parameters used to calculate these plots are shown in Table 1.

complex amplitude E with angular frequency ω in a solid of band gap U and reduced electron-hole mass m_r is:¹⁸

$$W_{\text{PI}}(|E|, \omega, U, m_r) = \frac{2\omega}{9\pi} \left(\frac{m_r \omega}{\sqrt{\gamma_1} \hbar} \right)^{3/2} Q(\gamma, x) \exp(-\varpi \langle x + 1 \rangle). \quad (1)$$

Here the Keldysh parameter $\gamma = \omega \sqrt{m_r U} / e |\xi|$, $\gamma_1 = \gamma^2 / (1 + \gamma^2)$, $\varpi = \pi (K(\gamma_1) - E(\gamma_2)) / E(\gamma_2)$, $\gamma_2 = 1 - \gamma_1$, and $x = (2U/\pi\omega)(\sqrt{1 - \gamma^2}/\gamma)E(\gamma_2)$. The functions $K(x)$ and $E(x)$ are complete elliptical integrals of the first and second kind, respectively, as defined in Ref. 40. The function $Q(\gamma, x)$ is given by

$$Q(\gamma, x) = \sqrt{\frac{\pi}{2K(\gamma_2)}} \sum_{n=0}^{\infty} \exp(-n\varpi) \Phi\left(\sqrt{\vartheta(n+2\nu)}\right),$$

where $\vartheta = \pi^2/4K(\gamma_2)E(\gamma_2)$, $\nu = \langle x + 1 \rangle - x$, $\langle \cdot \rangle$ denotes the integer part, and $\Phi(z) = \int_0^z \exp(y^2 - z^2) dy$ is the Dawson function. In this work, an approximate multi-chromatic photoionization rate is calculated by using the instantaneous frequency $\omega(t) = \Im[(\partial_t E)/E]$ in Eq. (1), where the notation $\Im[\cdot]$ denotes the imaginary part and E is the complex electric field. For the case of a negatively-chirped laser pulse, the blue-shifted photons on the leading pulse edge lead to higher photoionization rates earlier in the laser pulse, giving more time for impact ionization to raise the total ionization yield. The opposite situation occurs for a positively-chirped laser pulse, where red-shifted photons on the leading pulse edge lowers the photoionization rate there, giving less time for impact ionization. The importance of this effect was verified experimentally when it was shown that the surface damage threshold for fused silica was up to 20% lower for a negatively-chirped ultrashort laser pulse, as compared to that of an otherwise identical positively-chirped pulse.³²

Using the instantaneous frequency in the Keldysh formula allows us to model the effect of a changing average pulse frequency, which occurs naturally during nonlinear propagation due to self-phase modulation. Figure 1 shows how even small changes in the average frequency can lead to order-of-magnitude changes in the photoionization rate in the MPI regime. Note that although the rate generally increases as wavelength decreases, a blue-shifted frequency will initially see reduction in the total rate until a transition wavelength occurs, indicating that one fewer photon is needed for ionization, at which point the rate increases by an order of magnitude. The opposite case occurs with red shifted frequencies. Using the instantaneous frequency in the Eq. 1 naturally captures this behavior.

2.2 Laser-Material Dynamics Model

In an earlier work,⁴¹ our results demonstrated that coupling pulse propagation to a carrier energy-resolved model originally developed for semiconductors¹⁰ potentially holds much higher predictive ability than the simplified, monochromatic rate equation models for the free carrier density. In Ref. 41, high-intensity pulse propagation in bulk fused silica results in self-phase modulation at the beam center, broadening the on-axis pulse spectrum (super-continuum generation) and chirping the pulse in time. This is the case even for ultrafast pulses that are initially transform-limited and thus well-described by the monochromatic approximation. To account for this

fact, we model the laser-induced ionization and resulting conduction band dynamics using an extended multi-rate-equation (MRE)¹⁰ that discretizes the carrier distribution in energy-space. We account for the broadband nature of the pulses in the Keldysh photoionization model¹⁸ and the extended MRE model using the instantaneous pulse frequency at each point in space and time as opposed to the central laser frequency. The extended MRE comprises carrier populations at incremental values in energy space:

$$\begin{aligned} \frac{d}{dt}n(\epsilon_i, t) = & W_{\text{PI}}(t)\delta_{\epsilon_i, \epsilon_{\text{PI}}} + [W^{1pt}(\epsilon_i - \hbar\omega(t), t) - W^{1pt}(\epsilon_i, t)] \\ & + \left[\frac{n(\epsilon_i + \epsilon_{pn}, t)}{\tau^{pn}(\epsilon_i + \epsilon_{pn})} - \frac{n(\epsilon_i, t)}{\tau^{pn}(\epsilon_i)}\theta(\epsilon_i - \epsilon_{pn}) \right] - \frac{n(\epsilon_i, t)}{\tau_d(\epsilon_i)} \\ & + \left[\sum_{l=j}^m \alpha(\epsilon_l)n(\epsilon_l)\delta_{i, l+1} + \alpha(\epsilon_i + \epsilon_c)n(\epsilon_i + \epsilon_c, t) - \alpha(\epsilon_i)n(\epsilon_i, t)\theta(\epsilon_i - \epsilon_c) \right], \end{aligned} \quad (2)$$

where ϵ_i is the ‘ i^{th} ’ represented conduction-band energy and $n(\epsilon_i, t)$ is the density of free carriers in the energy range $\epsilon_{i+1} - \epsilon_i$. The terms on the right-hand side represent from left to right: a photoionization contribution where $\epsilon_{\text{PI}} = \left\langle \frac{\tilde{\Delta}}{\hbar\omega(t)} + 1 \right\rangle \hbar\omega(t) - \tilde{\Delta}$ is the energy at which a photo-ionized electrons enter the conduction band, $\tilde{\Delta}$ is the effective band gap, and $\omega(t)$ is the instantaneous frequency. The free-carrier absorption contributions $W^{1pt}(\epsilon_i - \hbar\omega(t), t)$ and $W^{1pt}(\epsilon_i, t)$ represent electrons entering or exiting (respectively) the carrier population at energy ϵ_i by 1-photon absorption events. Electron energy relaxation into the lattice is represented in the middle line where $\tau^{pn}(\epsilon_i)$ is the energy dependent phonon scattering time and ϵ_{pn} is the mean phonon energy. The process of impact ionization is modeled on the last line where $\alpha(\epsilon_l)$ is the impact-ionization coefficient, ϵ_c is the critical energy for impact ionization, and $\theta(x)$ is the Heaviside step function.¹⁰ The formulas to calculate $\tilde{\Delta}$, ϵ_c are taken from Ref. 17. The avalanche contribution allows electrons with energy exceeding ϵ_c to impact a valance electron and promote it to the conduction band, losing an energy equal to the band gap U in the process. The energy dependence of the impact ionization rate $\alpha(\epsilon_i)$ is given by the Keldysh impact ionization formula $\alpha_i = P((\epsilon_i - \epsilon_c)/\epsilon_c)^2 \theta(\epsilon_i - \epsilon_c)$. This work assumes that the rate coefficient $P = 21.2 \text{ fs}^{-1}$, which is also taken from Ref. 17.

The evolution of the free current density entering the Maxwell equations is coupled to the electron plasma, and is identically discretized in energy space. In this work, an extended MRE for a Drude free current density \vec{J}_f for electrons of energy ϵ_i is solved simultaneously with the extended MRE:

$$\frac{d}{dt}\vec{J}_f(\epsilon_i, t) = -\frac{\vec{J}_f(\epsilon_i, t)}{\tau^{pn}(\epsilon_i)} + \frac{e^2}{m(\epsilon_i)}n(\epsilon_i, t)\vec{E}(t), \quad (3)$$

where $m(\epsilon_i)$ is the effective mass. This allows the calculation of optical contributions from electrons in every electron-energy region represented in the simulations. The time-average of the quantity $\vec{J}_f(\epsilon_i, t) \cdot \vec{E}(t)$ is used to determine the one-photon absorption contributions to Eq. 2:

$$W^{1pt}(\epsilon_i, t) = \frac{[\vec{J}_f(\epsilon_i, t) \cdot \vec{E}(t)]_{\text{avg}}}{\hbar\omega(t)}.$$

The sum over all energies then gives the total plasma density, as well as the free current density for use in the propagation model; see Sec. 2.3.

2.3 Ultrashort Pulse Propagation Model

The above models of ionization and laser-plasma dynamics are used to simulate ultrashort laser pulse propagation through, and initiating induced modification in, bulk fused silica. The ionization models are compatible with the most common and current models of pulse propagation; including envelope equations for the complex electric field amplitude,⁴² spectral methods,⁴³ unidirectional pulse propagation equations (UPPEs),⁴⁴ and Finite-Difference

Time-Domain (FDTD) methods. The primary method for modeling the pulse propagation in this work will be solving a UPPE for the electric field:⁴⁵

$$\partial_z E_{k_x, k_y}(\omega, z) = ik_z E_{k_x, k_y} + \frac{i\omega^2}{2\epsilon_0 c^2 k_z} P_{k_x, k_y}(\omega, z) + \frac{i\omega}{2\epsilon_0 c^2 k_z} J_{k_x, k_y}(\omega, z). \quad (4)$$

Here E is the forward propagating component of the electric field, z is the propagation axis, ω is the angular frequency, k_x and k_y are the transverse beam coordinates, P is the nonlinear polarization, J is the free current density, $\epsilon(\omega)$ is the linear electric permittivity, and $k_z = \sqrt{\omega\epsilon(\omega)/c + k_x^2 + k_y^2}$. Note that this is a fully spectral method solving for the analytic (*i.e.* forward propagating) electric field as it evolves along the propagation axis. In this method, there is no reference to a field envelope or a constant carrier frequency. The ionization models above are also free of this assumption, relying as they do on the instantaneous frequency. The right-hand side of Eq. 4 contains linear optical contributions of dispersion and diffraction, including all high-order dispersion as well as linear and nonlinear-shock formation. The nonlinear polarization term includes the Kerr effect while the current density term includes photoionization and plasma effects.

For simulations, Eq. (4) is transformed into the retarded time frame of the laser pulse for propagation over long distances through the bulk. The material response in Equation (4) is contained in the linear permittivity function $\epsilon(\omega)$, the nonlinear polarization, and the current density. We use a Sellmeier equation to calculate $\epsilon(\omega)$ in the spectral domain. The polarization and current density are calculated in the space-time domain and then Fourier transformed into the spectral (k - ω) domain. The nonlinear polarization is assumed to be of a standard Kerr type: $P(t) = \epsilon_0 \chi^{(3)} E(t)^3$, where $\chi^{(3)}$ is related to the nonlinear refractive index n_2 by $\chi^{(3)} = (4/3)n_2\epsilon_0 c n_0^2$. Note that, unlike standard envelope treatments, this polarization allows for third harmonic generation as well as cascaded high-order harmonic generation.⁸ Later we will show how this feature eventually limits the applicability of the instantaneous frequency to the ionization models above, at which point a strictly intensity-dependent nonlinear polarization given by $P(t) = \epsilon_0 3\chi^{(3)} |E|^2 E(t)$ should be used. The current density has two contributions. The first is the free current density, calculated by solving and then summing Eq. 3 over all carrier energies. The second contribution comes from a photoionization current which is calculated by $J_{PI}(t) = n_0 \epsilon_0 c E(t) W_{PI}(t) U / 2I$, where I is the field intensity and the photoionization rate $W_{PI}(t)$ is given by Eq. 1 using the instantaneous frequency. For a detailed tutorial on how Eq. 4 is derived and is best solved numerically we refer the reader to Ref. 8.

Table 1. Numerical values used in all the simulations reported in this work. Material parameters are those for fused silica.

<i>Symbol</i>	Description	Value	Units
λ	Initial wavelength	800	nm
τ_0	Initial pulsewidth ($1/e^2$)	84.9	fs
w_r	Initial beam width ($1/e^2$)	2	mm
E_n	Initial pulse energy	750	nJ
f	Lens focal length	25	cm
n_0	Linear refractive index	1.45	
n_2	Nonlinear refractive index	3×10^{-16}	cm^2W^{-1}
U	Material band gap	9	eV
m_e	Effective electron mass	9.11×10^{-31}	kg
m_r	Reduced electron-hole mass	4.56×10^{-31}	kg
τ_d	Electron-defect relaxation time	150	fs

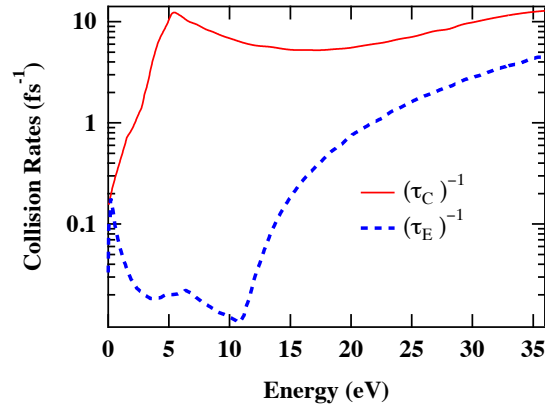


Figure 2. Electron-energy dependent collision rates in fused silica used for all simulations in this work.²⁹

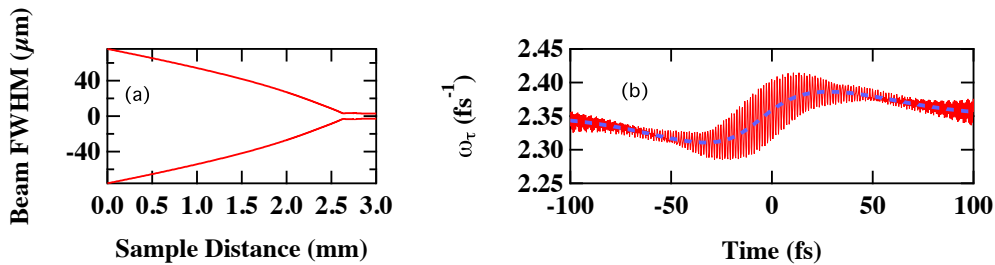


Figure 3. (a) The FWHM beam width of the pulse as it propagates through the sample. (b) The instantaneous frequency with (solid red line) and without (dashed blue line) high-harmonic generation included in the nonlinear polarization.

3. PULSE PROPAGATION SIMULATIONS

The simulations begin by constructing the forward propagating analytic electric field at the beginning of the propagation according to the formula

$$E(r, \tau, z = -f) = \sqrt{\frac{2I_0}{\epsilon_0 c}} \exp\left(-\frac{r^2}{w_r^2} - i\frac{k_0 r^2}{2f} - \frac{\tau^2}{\tau_0^2}\right),$$

where $I_0 = E_n/(\pi/2)^{3/2}\omega_r^2\tau_0$ is the initial peak intensity, and all other parameters are defined in Table 1. The geometric focus of the laser beam is placed 3 mm into the bulk of a fused silica sample to preclude any surface damage effects. The pulse is numerically focused into the fused silica by solving the UPPE simultaneously with the coupled extended multi-rate equations.

The energy-dependent electron momentum and energy relaxation (collision) times used in the extended MREs are taken from Ref. 29 and are shown in Fig. 2. Note that these values vary by many orders of magnitude over the electron energy range. Note also that in Refs. 17 and 29, parabolic band structure is assumed with effective electron and hole masses equal to the rest electron mass. For the sake of consistency, we make the same assumptions. Also, lacking a model for the energy dependence of the defect-relaxation time τ_d , we assume a constant value of 150 fs.^{13,14} Due to the ultrashort time scales of exposure, defects will not play a major role in either the propagation or the plasma generation.

Pulse propagation simulations are performed under these conditions for four cases and are organized by the methods of calculating the nonlinear polarization and the ‘instantaneous’ frequency as follows:

(1) $P(t) = \epsilon_0\chi^{(3)}E(t)^3$ and $\omega(t) = \Im[(\partial_t E)/E]$; (2) $P(t) = \epsilon_0\chi^{(3)}E(t)^3$ and $\omega(t) = \omega_0$; (3) $P(t) = \epsilon_03\chi^{(3)}|E|^2 E(t)$ and $\omega(t) = \Im[(\partial_t E)/E]$; (4) $P(t) = \epsilon_03\chi^{(3)}|E|^2 E(t)$ and $\omega(t) = \omega_0$, where $\omega_0 = 2\pi c/\lambda$. Although the geometric focus is located at 3 mm into the sample, note that Fig. 3a shows that the pulse comes to a nonlinear focus

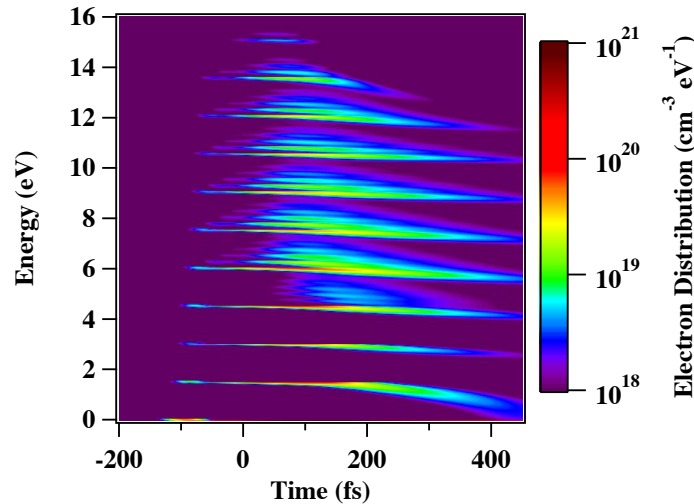


Figure 4. Solutions to the extended MRE as a function of conduction band energy and time. The incident pulse train comprised a 50 fs, 267 nm pulse of peak intensity 2×10^{12} W/cm², followed by a 150 fs, 800 nm pulse of peak intensity 1×10^{13} W/cm². The peaks of the two pulses were separated by 100 fs.

earlier due to self-focusing. The resulting peak plasma generation in the sample is recorded as a function of propagation distance starting just before the nonlinear focus. Fig. 3b shows the instantaneous frequency at the beam center just prior to the nonlinear focus at $z = 2.5$ mm for cases (1) and (3). The periodic instability in the red line come primarily from third harmonic generation (THG). After the nonlinear focus is reached the values of the instantaneous frequency in case (1) become non-physical, and the simulation breaks down at approximately 2.75 mm of propagation in the sample. The other cases, however, continued without difficulty. These results indicate that in the presence of multiple distinct spectral peaks the instantaneous frequency should not be used. However, note that if THG is omitted as in case (3), it remains valid.

4. TWO-PULSE PLASMA GENERATION SIMULATIONS

In order to numerically propagate a pulse that experiences high harmonic generation and plasma generation simultaneously, the instantaneous frequency cannot be used as a meaningful input value to the material models. Once the high harmonic fields are large enough to interfere noticeably with the fundamental, a different method can be used. If one filters out each harmonic signal individually in frequency space and separately transforms them back into the time domain, one can solve Equations 2 and 3 using a split-step technique; one split-step for each harmonic frequency. In isotropic media this will typically require only the first and third harmonics. In surface structuring studies of fused silica there is increasing interest in seeding laser-induced ionization with a UV pulse followed by a near-IR pulse to drive avalanching.^{13,14} In such cases the delay between the two pulses is often short enough that the two fields are present at the same and time, as they would also be in bulk co-propagation as the pulses pass through one another.

To demonstrate this method, we solve Equations 2 and 3 for a pulse train consisting of a 267 nm, 50 fs pulse followed by an 800 nm, 150 fs pulse. The 800 nm pulse is assigned a peak intensity of 1×10^{13} W/cm² and the 267 nm an intensity 20% of that of the 800 nm pulse. Note that, for identical beam conditions, this yields a UV pulse energy of only 6.7% that of the near IR pulse. By solving the extended MREs for multiple delay times, the maximum plasma density generated was approximately 2×10^{20} cm⁻³ and corresponded to a delay of 100 fs. When the extended MREs were solved for each pulse alone, the maximum plasma densities generated were both on the order of 2×10^{18} cm⁻³. Figure 4 show the solution to the extended MRE as a function of time and free-carrier energy. In this plot $t = 0$ corresponds to the center of the 800 nm pulse. The center of the 267 nm pulse is located at $t = -100$ fs. The multi-chromatic nature of the pulse train is well-captured in this model as shown by the evenly spaced energy levels for the 800 nm pulse, as well as the initial appearance

of distinct energy levels at three times that spacing. This technique should be substituted for the instantaneous frequency approach when high harmonics, or any appreciable frequency components strongly distinct from the fundamental are present.

5. CONCLUSION

Simulations have been performed using an energy-resolved extended multi-rate equation to model multi-chromatic laser-induced plasma generation in bulk fused silica for both single and different-frequency multi-pulse systems. This model was also coupled with a unidirectional pulse propagation equation to simulate single pulse propagation through the bulk. It was found that, to the extent that third harmonic generation is negligible, allowing the instantaneous frequency to play the role of the constant frequency in the traditional monochromatic plasma model is a robust and effective way of modeling the self-frequency shifts that naturally occur during propagation. However, appreciable harmonic generation in the dielectric results in non-physical behavior that bring the plasma calculation into question using this method. In circumstances where two pulses of different frequency are deliberately co-propagated, the extended multi-rate equation can be solved approximately using a split-step method. Our results predict that a 50 fs, 267 nm pulse followed by a more energetic 150 fs, 800 nm pulse generates a plasma density two orders of magnitude greater than either pulse generates alone. Further studies are expected to reveal exploitable multi-chromatic plasma generation in both surface and bulk laser-machining of solids.

ACKNOWLEDGMENTS

This work was supported by the Air Force Office for Scientific Research under grant FA9550-13-1-0069.

REFERENCES

- [1] Zhu, X., Naumov, A., Villeneuve, D., and Corkum, P., "Influence of laser parameters and material properties on micro drilling with femtosecond laser pulses," *Appl. Phys. A* **V69**(0), S367–S371 (1999).
- [2] Schaffer, C. B., Brodeur, A., and Mazur, E., "Laser-induced breakdown and damage in bulk transparent materials induced by tightly focused femtosecond laser pulses," *Meas. Sci. Technol.* **12**, 1784–1794 (Nov 2001).
- [3] Bergé, L., Skupin, S., Nuter, R., Kasparian, J., and Wolf, J.-P., "Ultrashort filaments of light in weakly ionized, optically transparent media," *Rep. on Prog. in Phys.* **70**(10), 1633 (2007).
- [4] Vogel, A., Noack, J., Huttman, G., and Paltauf, G., "Mechanisms of femtosecond laser nanosurgery of cells and tissues," *Appl. Phys. B* **81**, 1015–1047 (Dec 2005).
- [5] Boyd, R. W., [*Nonlinear Optics*], Academic Press, 2nd ed. (Dec. 2002).
- [6] Diels, J.-C. and Rudolf, W., [*Ultrashort Laser Pulse Phenomena: Fundamentals, Techniques, and Applications on a Femtosecond Time Scale*], Academic Press, 2nd ed. (2006).
- [7] Kolesik, M., Whalen, P. T., and Moloney, J. V., "Theory and simulation of ultrafast intense pulse propagation in extended media," *IEEE J. Sel. Topics. Quantum Electron.* **18**, 494–506 (January/February 2012).
- [8] Couairon, A., Brambilla, E., Corti, T., Majus, D., de J. Ramírez-Góngora, O., and Kolesik, M., "Practitioner's guide to laser pulse propagation models and simulation," *The European Physical Journal - Special Topics* **199**, 5–76 (2011). 10.1140/epjst/e2011-01503-3.
- [9] Stuart, B. C., Feit, M. D., Herman, S., Rubenchik, A. M., Shore, B. W., and Perry, M. D., "Nanosecond-to-femtosecond laser-induced breakdown in dielectrics," *Phys. Rev. B* **53**, 1749–1761 (Jan 1996).
- [10] Medvedev, N. and Rethfeld, B., "A comprehensive model for the ultrashort visible light irradiation of semiconductors," *J. Appl. Phys.* **108**(10), 103112 (2010).
- [11] Rethfeld, B., "Free-electron generation in laser-irradiated dielectrics," *Phys. Rev. B* **73**(3), 035101 (2006).
- [12] Rethfeld, B., "Unified model for the free-electron avalanche in laser-irradiated dielectrics," *Phys. Rev. Lett.* **92**(18), 187401 (2004).
- [13] Yu, X., Bian, Q., Zhao, B., Chang, Z., Corkum, P. B., and Lei, S., "Near-infrared femtosecond laser machining initiated by ultraviolet multiphoton ionization," *Applied Physics Letters* **102**(10), 101111 (2013).

- [14] Yu, X., Bian, Q., Chang, Z., Corkum, P. B., and Lei, S., "Femtosecond laser nanomachining initiated by ultraviolet multiphoton ionization," *Opt. Express* **21**, 24185–24190 (Oct 2013).
- [15] Huang, D., Apostolova, T., Alsing, P. M., and Cardimona, D. A., "High-field transport of electrons and radiative effects using coupled force-balance and fokker-planck equations beyond the relaxation-time approximation," *Phys. Rev. B* **69**, 075214 (Feb 2004).
- [16] Huang, D., Alsing, P. M., Apostolova, T., and Cardimona, D. A., "Effect of photon-assisted absorption on the thermodynamics of hot electrons interacting with an intense optical field in bulk gaas," *Phys. Rev. B* **71**, 045204 (Jan 2005).
- [17] Kaiser, A., Rethfeld, B., Vicanek, M., and Simon, G., "Microscopic processes in dielectrics under irradiation by subpicosecond laser pulses," *Phys. Rev. B* **61**, 11437–11450 (May 2000).
- [18] Keldysh, L. V., "Ionization in the field of a strong electromagnetic wave," *Sov. Phys. JETP* **20**(5), 1307 (1965).
- [19] Perelomov, A. M., Popov, V. S., and Terent'ev, M. V., "Ionization of atoms in an alternating electric field: I," *Sov. Phys. JETP* **23**, 924 (1966).
- [20] Perelomov, A. M., Popov, V. S., and Terent'ev, M. V., "Ionization of atoms in an alternating electric field: II," *Sov. Phys. JETP* **24**, 207 (1967).
- [21] Holway, L. H., "High-frequency breakdown in ionic crystals," *J. Appl. Phys.* **45**(2), 677–683 (1974).
- [22] Holway, L. H. and Fradin, D. W., "Electron avalanche breakdown by laser radiation in insulating crystals," *J. Appl. Phys.* **46**(1), 279–291 (1975).
- [23] Sparks, M., Mills, D. L., Warren, R., Holstein, T., Maradudin, A. A., Sham, L. J., Loh, E., and King, D. F., "Theory of electron-avalanche breakdown in solids," *Phys. Rev. B* **24**, 3519–3536 (Sep 1981).
- [24] Couairon, A., Sudrie, L., Franco, M., Prade, B., and Mysyrowicz, A., "Filamentation and damage in fused silica induced by tightly focused femtosecond laser pulses," *Phys. Rev. B* **71**(12), 125435 (2005).
- [25] Gulley, J. R., Winkler, S. W., Dennis, W. M., Liebig, C. M., and Stoian, R., "Interaction of ultrashort-laser pulses with induced undercritical plasmas in fused silica," *Phys. Rev. A* **85**, 013808 (Jan 2012).
- [26] Gulley, J. R., Winkler, S. W., and Dennis, W. M., "Simulation and analysis of ultrafast-laser-pulse-induced plasma generation in fused silica," *Opt. Eng.* **47**(5), 054302 (2008).
- [27] Skupin, S. and Berge, L., "Self-guiding of femtosecond light pulses in condensed media: Plasma generation versus chromatic dispersion," *Physica D* **220**, 14–30 (Aug 2006).
- [28] Wu, A. Q., Chowdhury, I. H., and Xu, X., "Femtosecond laser absorption in fused silica: Numerical and experimental investigation," *Phys. Rev. B* **72**(8), 085128 (2005).
- [29] Arnold, D., Cartier, E., and DiMaria, D. J., "Acoustic-phonon runaway and impact ionization by hot electrons in silicon dioxide," *Phys. Rev. B* **45**(3) (1992).
- [30] Gulley, J. R., "Ultrafast laser-induced damage and the influence of spectral effects," *Opt. Eng.* **51**(12), 121805 (2012).
- [31] Gulley, J. R. and Dennis, W. M., "Ultrashort-pulse propagation through free-carrier plasmas," *Phys. Rev. A* **81**, 033818 (Mar 2010).
- [32] Louzon, E., Henis, Z., Pecker, S., Ehrlich, Y., Fisher, D., Fraenkel, M., and Zigler, A., "Reduction of damage threshold in dielectric materials induced by negatively chirped laser pulses," *Appl. Phys. Lett.* **87**(24), 241903 (2005).
- [33] Berge, L., Skupin, S., and Steinmeyer, G., "Temporal self-restoration of compressed optical filaments," *Phys. Rev. Lett.* **101**(21), 213901 (2008).
- [34] Sudrie, L., Couairon, A., Franco, M., Lamouroux, B., Prade, B., Tzortzakis, S., and Mysyrowicz, A., "Femtosecond laser-induced damage and filamentary propagation in fused silica," *Phys. Rev. Lett.* **89**, 186601 (Oct 2002).
- [35] Winkler, S. W., Burakov, I. M., Stoian, R., Bulgakova, N. M., Husakou, A., Mermillod-Blondin, A., Rosenfeld, A., Ashkenasi, D., and Hertel, I. V., "Transient response of dielectric materials exposed to ultrafast laser radiation," *Appl. Phys. A* **V84**(4), 413–422 (2006).
- [36] Christensen, B. H. and Balling, P., "Modeling ultrashort-pulse laser ablation of dielectric materials," *Phys. Rev. B* **79**(15), 155424 (2009).

- [37] Liu, J., Li, R., and Xu, Z., “Few-cycle spatiotemporal soliton wave excited by filamentation of a femtosecond laser pulse in materials with anomalous dispersion,” *Phys. Rev. A* **74**(4), 043801 (2006).
- [38] Mero, M., Liu, J., Rudolph, W., Ristau, D., and Starke, K., “Scaling laws of femtosecond laser pulse induced breakdown in oxide films,” *Phys. Rev. B* **71**(11), 115109 (2005).
- [39] Polesana, P., Dubietis, A., Porras, M. A., Kucinskas, E., Faccio, D., Couairon, A., and Trapani, P. D., “Near-field dynamics of ultrashort pulsed bessel beams in media with kerr nonlinearity,” *Phys. Rev. E* **73**(5), 056612 (2006).
- [40] Abramowitz, M. and Stegun, I. A., [*Handbook of Mathematical Functions*], Dover, New York, tenth ed. (1964).
- [41] Gulley, J. R., “Modeling free-carrier absorption and avalanching by ultrashort laser pulses,” *Laser-Induced Damage in Optical Materials: 2011* **8190**, 819022, SPIE (2011).
- [42] Brabec, T. and Krausz, F., “Nonlinear optical pulse propagation in the single-cycle regime,” *Phys. Rev. Lett.* **78**, 3282–3285 (Apr 1997).
- [43] Kinsler, P., Radnor, S. B. P., and New, G. H. C., “Theory of directional pulse propagation,” *Phys. Rev. A* **72**, 063807 (Dec 2005).
- [44] Kolesik, M., Moloney, J. V., and Wright, E. M., “Polarization dynamics of femtosecond pulses propagating in air,” *Phys. Rev. E* **64**, 046607 (Sep 2001).
- [45] Kolesik, M. and Moloney, J. V., “Nonlinear optical pulse propagation simulation: From Maxwell’s to unidirectional equations,” *Phys. Rev. E* **70**, 036604 (Sep 2004).